RESEARCH ARTICLE

Heat Transportation During Slip Flow of Non-Newtonian Rheology with Thermal Stratification past a Stretched Surface

Hashim[1,*], **Kashif Mehmood**[1] **and Bilal Sher Afzal**[1]

[1] Department of Mathematics and Statistics, University of Haripur, Haripur 22620, Pakistan

Abstract

This study investigates heat transportation in slip flow of a non-Newtonian fluid with thermal stratification over a stretched surface, a configuration that closely represents many industrial and engineering processes. The inclusion of slip effects and non-Newtonian rheology provides a more realistic description of flows encountered in polymer extrusion, coating technologies, micro- and nano-scale devices, and biomedical systems. Thermal stratification is incorporated to model non-uniform temperature environments commonly observed in heat exchangers, cooling of electronic components, and energy systems. The governing partial differential equations for momentum, energy, and nanoparticle concentration are transformed into a system of nonlinear ordinary differential equations using appropriate similarity transformations. The resulting boundary value problem is solved numerically to analyze the impact of key parameters such as the slip coefficient, thermal stratification parameter, Sutterby fluid parameter, and Brownian motion on velocity, temperature, and concentration profiles. Results indicate that thermal stratification significantly reduces the temperature distribution within the boundary layer, while velocity slip at the surface diminishes the skin friction coefficient. The non-Newtonian characteristics of the Sutterby fluid substantially influence the heat transfer rate, with shear-thinning fluids demonstrating enhanced thermal performance compared to shear-thickening fluids. This analysis provides valuable insights for thermal engineering applications involving non-Newtonian nanofluids in stratified environments.

Keywords: non-Newtonian Sutterby model, nanofluids, thermal stratification, buongiorno's model, heat transport.

1 Introduction

The importance of nanofluids lies in their revolutionary ability to enhance thermal conductivity and heat transfer efficiency beyond the limits of traditional fluids. This capability is paramount for advanced technological applications, ranging from the thermal management of microchips and energy systems like solar collectors to specialized uses in biomedicine

Submitted: 01 September 2025
Accepted: 25 February 2026
Published: 28 March 2026

Vol. 2, **No.** 1, 2026.
10.62762/IJTSSE.2025.505390

***Corresponding author:**
Hashim
hashim@uoh.edu.pk

Citation
Hashim, Mehmood, K., & Afzal, B. S. (2026). Heat Transportation During Slip Flow of Non-Newtonian Rheology with Thermal Stratification past a Stretched Surface. *International Journal of Thermo-Fluid Systems and Sustainable Energy*, 2(1), 18–29.

and materials processing. Consequently, nanofluids represent a fundamental enabling technology for pushing the boundaries of performance in modern thermal engineering. The pursuit of enhanced thermal performance in engineering systems has been significantly advanced by the introduction of nanofluids, a concept pioneered by Choi [1] in his seminal work, which demonstrated that the suspension of nanoparticles in a base fluid drastically improves its thermal conductivity. Building on this foundational discovery, Xuan et al. [2] further explored the convective heat transfer capabilities of nanofluids, establishing their potential beyond mere conductivity enhancement. A critical theoretical framework was later established by Buongiorno [3], whose model identified Brownian motion and thermophoresis as the primary mechanisms for energy transport in nanofluids, providing a robust two-component non-homogeneous equilibrium model that has become a standard in the field. This model enabled the systematic study of nanofluids in various boundary layer configurations. For instance, Kuznetsov et al. [4] analytically investigated natural convective flow past a vertical plate, while Makinde et al. [5] studied a stretching sheet with a convective boundary condition, a more realistic thermal scenario. The complexity was extended to stagnation point flows by Mostafa et al. [6] and further to magnetohydrodynamic (MHD) stagnation point flow by Ibrahim et al. [7]. Hamad et al. [8] computed the similarity solution for stagnation point flow past a heated porous stretching surface with nanofluid and heat transport analysis. The thermal performance of nanofluids in boundary layer flows has been extensively explored, beginning with fundamental configurations such as flow between non-parallel stretching walls [9]. Research has progressively incorporated greater physical complexity, including magnetohydrodynamics (MHD), second-order slip, and melting heat transfer [10]. The advent of hybrid nanofluids marked a significant advancement, with studies directly comparing their superior thermal efficacy against conventional nanofluids under the influence of viscous dissipation [11] and thermal radiation [12]. Very recently, the focus has shifted toward more sophisticated scenarios involving non-Newtonian nanofluids over curved surfaces [13] and thermodynamic analysis of bio-inspired fluids with interface slip and melting phenomena [14]. Some recent works in this direction are presented in works [15–22].

The classical no-slip boundary condition, a cornerstone of macro-scale fluid dynamics, becomes increasingly invalid in a host of modern applications, necessitating the incorporation of slip models for accurate physical representation [26]. Such conditions are paramount in micro- and nano-scale systems (MEMS/NEMS), where the characteristic length scales are small, in rarefied gas flows, and for certain non-Newtonian fluids. The foundational work on this subject was pioneered by Andersson [23] and Wang [24], who provided exact analytical solutions for slip flow past a stretching surface and a moving plate, respectively, thereby establishing a critical theoretical baseline. The modeling of slip itself has evolved significantly, progressing from first-order models to more physically comprehensive second-order and non-linear frameworks. For instance, Wu [25] developed a generalized slip model valid across a wide range of Knudsen numbers, while Fang et al. [27] and Hayat et al. [28] implemented second-order slip and non-linear Navier boundary conditions to capture more intricate near-wall dynamics in viscous flows over stretching and shrinking sheets. The interplay between slip and magnetohydrodynamics (MHD) further enriches this field, as explored in the exact solutions for MHD slip flow by Aziz et al. [29] and the analyses of flows over permeable stretching sheets under MHD and slip effects by Fang et al. [30]. The thermal implications are equally critical, with studies like Nandeppanavar et al. [31] investigating the concomitant effects of hydrodynamic and thermal slip under a constant heat flux boundary condition. The relevance of slip extends directly into nanofluid research, where Turkyilmazoglu [32] derived exact solutions for heat and mass transfer in MHD slip flow of nanofluids, and other researchers have integrated slip with phenomena like heat generation/absorption and convective boundary conditions [33].

This study presents a comprehensive analysis of heat and nanoparticle transport in slip flow of a non-Newtonian Sutterby nanofluid over a stretching surface under thermal stratification. The novelty lies in the combined investigation of velocity and thermal slip effects with non-Newtonian rheology, capturing realistic flow behavior in industrial and micro/nanoscale applications. Thermal stratification and heat generation/absorption are incorporated to model non-uniform temperature environments, while the impact of key parameters-such as slip coefficients, Sutterby fluid parameters, and Brownian motion-on velocity, temperature, and concentration profiles is systematically analyzed. Furthermore, the study demonstrates that the shear-thinning nature of the Sutterby fluid significantly enhances thermal transport, providing practical insights for optimizing heat transfer and process control in advanced thermal engineering systems.

2 Model Development

The physical model under consideration is depicted in Figure 1. It involves a steady, two-dimensional, incompressible flow of a non-Newtonian Sutterby nanofluid over a continuously stretching flat surface. The surface is stretched with a linear velocity defined by $u_w(x) = ax$, where $a > 0$ is a constant stretching rate.

This analysis incorporates several physical complexities to enhance the realism of the model.

- The flow is subject to velocity slip at the boundary, acknowledging its significance in micro-scale or specific rheological contexts.
- Heat transfer is modeled by including the effects of non-linear thermal radiation and internal heat generation/absorption.
- A key aspect of this study is the investigation of thermal stratification on both temperature and concentration fields, for which the wall temperature is $T_w(x) = T_0 + m_1 x$ and the temperature far away from the plate is $T_\infty(x) = T_0 + m_2 x$.
- On the other hand, **solutal** stratification is also included with wall concentration $C_w(x) = C_0 + m_3 x$ and an ambient concentration $C_\infty(x) = C_0 + m_4 x$, where m_1, m_2, m_3, m_4 are the respective stratification parameters.

2.1 Non-Newtonian constitutive model

The Cauchy stress tensor for an **incompressible Sutterby fluid** is given by the following constitutive relationship [34]:

$$\tau = -pI + \mu S \tag{1}$$

where S is the extra stress tensor, defined as:

$$S = \mu_0 \left[\frac{\sinh^{-1}(B\hat{\gamma})}{(B\hat{\gamma})} \right]^n A_{1,\hat{\gamma}} \tag{2}$$

Here, μ_0 represents the dynamic viscosity, B is a material parameter, n is the power-law index, and $A_{1,\hat{\gamma}}$ is the first Rivlin-Ericksen tensor. The shear rate $\hat{\gamma}$ is expressed as:

$$\hat{\gamma} = \sqrt{\frac{1}{2}\operatorname{tr}(A_{1,\hat{\gamma}})^2} \tag{3}$$

Applying a second-order approximation for the inverse hyperbolic sine function:

$$\sinh^{-1}(B\hat{\gamma}) \approx B\hat{\gamma} - \frac{[B(\hat{\gamma})]^3}{6} \tag{4}$$

Hence, the extra stress tensor simplifies to:

$$S = \mu_0 \left[1 - \frac{B^2(\hat{\gamma})^2}{6} \right]^n A_{1,\hat{\gamma}} \tag{5}$$

Considering a two-dimensional, steady-state velocity field $V = [u(x,y), v(x,y), 0]$, the shear rate becomes:

$$\dot{\gamma} = \left[2\left(\frac{\partial u}{\partial x}\right)^2 + \left(\frac{\partial u}{\partial y} + \frac{\partial v}{\partial x}\right)^2 + 2\left(\frac{\partial u}{\partial y}\right)^2 \right]^{\frac{1}{2}} \tag{6}$$

The individual components of the extra stress tensor are:

$$S_{xx} = -P + 2\mu_0 \left[1 - \frac{B^2(\hat{\gamma})^2}{6} \right]^n \frac{\partial u}{\partial x} \tag{7}$$

$$S_{xy} = \mu_0 \left[1 - \frac{B^2(\hat{\gamma})^2}{6} \right]^n \left(\frac{\partial u}{\partial y} + \frac{\partial v}{\partial x} \right) \tag{8}$$

$$S_{yy} = -P + 2\mu_0 \left[1 - \frac{B^2(\hat{\gamma})^2}{6} \right]^n \frac{\partial v}{\partial y} \tag{9}$$

Employing the **Boussinesq approximations** and incorporating the **Buongiorno model** for nanofluids, the basic equations for momentum, energy, and concentration are derived as follows:

Continuity

$$\frac{\partial u}{\partial x} + \frac{\partial v}{\partial y} = 0, \tag{10}$$

Momentum

$$\begin{aligned} u\frac{\partial u}{\partial x} + v\frac{\partial u}{\partial y} &= \nu \left[1 - \frac{B^2}{6}\left(\frac{\partial u}{\partial y}\right)^2 \right]^n \left[\frac{\partial^2 u}{\partial y^2} \right] \\ &- \frac{n\nu B^2}{3} \left[1 - \frac{B^2}{6}\left(\frac{\partial u}{\partial y}\right)^2 \right]^{n-1} \\ &\times \left(\frac{\partial u}{\partial y}\right)^2 \left(\frac{\partial^2 u}{\partial y^2}\right) - \frac{\sigma B_0^2}{\rho_f} u, \end{aligned} \tag{11}$$

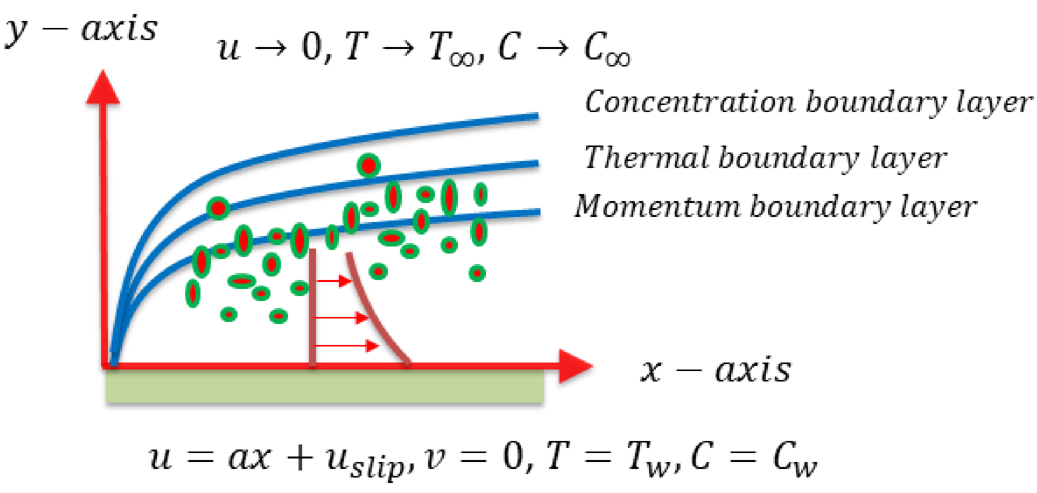

Figure 1. Physical interpretation of flow geometry.

Energy

$$u\frac{\partial T}{\partial x} + v\frac{\partial T}{\partial y} = \alpha\left(\frac{\partial^2 T}{\partial y^2}\right) - \frac{1}{(\rho c_p)_f}\left(\frac{16\sigma^* T_\infty^3}{3k^*}\frac{\partial^2 T}{\partial y^2}\right) + \frac{(\rho c_p)_p}{(\rho c_p)_f}\left[D_B\left(\frac{\partial C}{\partial y}\frac{\partial T}{\partial y}\right) + \frac{D_T}{T_\infty}\left(\frac{\partial T}{\partial y}\right)^2\right] + \frac{Q^*(T - T_\infty)}{(\rho c_p)_f}, \tag{12}$$

Concentration

$$u\frac{\partial C}{\partial x} + v\frac{\partial C}{\partial y} = D_B\left(\frac{\partial^2 C}{\partial y^2}\right) + \frac{D_T}{T_\infty}\left(\frac{\partial^2 T}{\partial y^2}\right), \tag{13}$$

Boundary Conditions

$$\text{at } y = 0: \quad u = u_w + L\left[1 - \frac{B^2}{6}\left(\frac{\partial u}{\partial y}\right)^2\right]^{n-1}\left(\frac{\partial u}{\partial y}\right),$$
$$v = 0, \quad T = T_w, \quad C = C_w,$$
$$\text{as } y \to \infty: \quad u \to U_\infty = 0, \quad T \to T_\infty, \quad C \to C_\infty. \tag{14}$$

2.2 Transformations

To make the governing system dimensionless, the following similarity variables are introduced:

$$\eta = \sqrt{\frac{a}{\nu}}\,y, \quad \psi = \sqrt{a\nu x}\,f(\eta),$$
$$\theta(\eta) = \frac{T - T_\infty}{T_w - T_0}, \quad \varphi(\eta) = \frac{C - C_\infty}{C_w - C_0} \tag{15}$$

where $f(\eta)$, $\theta(\eta)$, and $\varphi(\eta)$ represent the dimensionless stream function, temperature, and concentration, respectively.

Applying these transformations, Equations (10)–(15) reduce to the following system of coupled ordinary differential equations:

$$\left[1 - \frac{1}{6}De\,Re\,f''^2\right]f''' - \frac{1}{3}n\,De\,Re\left[1 - \frac{1}{6}De\,Re\,f''^2\right]^{n-1} f''^2 f''' - f'^2 + ff'' - Mf' = 0, \tag{16}$$

$$\left(1 + \frac{4}{3}R\right)\theta'' + Pr\left(Nb\,\varphi'\theta' + Nt\,\theta'^2 + f\theta' - f'\theta - s_t f' + Q\theta\right) = 0, \tag{17}$$

$$\varphi'' + Le\,f\varphi' - Le\,\varphi f' - Le\,s_c f' + \frac{Nt}{Nb}\theta'' = 0. \tag{18}$$

The transformed boundary conditions are:

$$f(0) = 0, \quad f'(0) = 1 + Af''(0)\left[1 - \frac{De\,Re\,f''^2(0)}{6}\right]^n, \tag{19}$$

$$\theta(0) = 1 - s_t, \quad \varphi(0) = 1 - s_c \quad \text{at } \eta = 0, \tag{20}$$

and as $\eta \to \infty$:

$$f'(\infty) \to 0, \quad \theta(\infty) \to 0, \quad \varphi(\infty) \to 0. \tag{21}$$

Here, the prime denotes differentiation with respect to η. The dimensionless parameters are the Deborah number De, heat generation/absorption parameter

Q, thermal stratification parameter s_t, and solutal stratification parameter s_c, defined as:

$$De = a^2B^2, \quad Q = \frac{Q^*}{a\rho c_p}, \quad s_t = \frac{m_2}{m_1}, \quad s_c = \frac{m_4}{m_3}. \tag{22}$$

The quantities of practical interest—skin friction coefficient C_f, Nusselt number Nu_x, and Sherwood number Sh_x—are given by:

$$\begin{aligned} Re^{\frac{1}{2}}C_f &= f''(0)\left[1 - \frac{1}{6}De\,Re\,f''^2(0)\right]^n, \\ Re^{-\frac{1}{2}}Nu_x &= -\left(\frac{1}{1-s_t}\right)\theta'(0), \\ Re^{-\frac{1}{2}}Sh_x &= -\left(\frac{1}{1-s_c}\right)\varphi'(0). \end{aligned} \tag{23}$$

3 Numerical Method

The exact solutions of formulated equations are not possible due to their highly nonlinear nature. As a result, a numerical method can be employed to find numerical solution for such problems. This will be done by converting the current governing problem (16)–(18) into a set of first-order equations. Here, we introduce the variables:

$$\begin{aligned} &f = z_1, \quad f' = z_2, \quad f'' = z_3, \quad \theta = z_4, \\ &\theta' = z_5, \quad \varphi = z_6, \quad \varphi' = z_7. \end{aligned} \tag{24}$$

This yields the following equivalent system:

$$\begin{cases} z_1' = z_2, \\ z_2' = z_3, \\ z_3' = \dfrac{z_2^2 - z_1z_3 + Mz_2}{A_1 - \left(\frac{1}{3}\right)nDeReA_2z_3}, \\ z_4' = z_5, \\ z_5' = -\dfrac{Pr\left(Nbz_5z_7 + Ntz_5^2 + z_1z_5 - z_2z_4 - z_2s_t + Qz_4\right)}{\left(1 + \frac{4}{3}R\right)}, \\ z_6' = z_7, \\ z_7' = -Lez_1z_7 + Lez_2z_6 + Les_cz_2 - \dfrac{Nt}{Nb}z_5', \end{cases} \tag{25}$$

subject to the boundary conditions:

$$\begin{aligned} &z_1(0) = 0, \quad z_2(0) = 1 + Az_3(0)\left[1 - \left(\frac{1}{6}\right)DeRe\,z_3^2(0)\right]^n, \\ &z_4(0) = 1 - s_t, \quad z_6(0) = 1 - s_c, \\ &z_2(\infty) \to 0, \quad z_4(\infty) \to 0, \quad z_6(\infty) \to 0. \end{aligned} \tag{26}$$

The governing system of nonlinear ordinary differential equations, given by equations (24)–(25), is solved numerically using the `bvp4c` solver in MATLAB, which is specifically designed for boundary value problems. This solver employs a collocation method based on the three-stage Lobatto IIIa formula, a fourth-order implicit Runge-Kutta scheme that ensures high accuracy and stability for stiff and nonlinear problems. To apply the far-field asymptotic boundary conditions, the semi-infinite domain is truncated at a sufficiently large value, $\eta_\infty = 10$, where the velocity, temperature, and concentration approach their ambient values. The solution process begins with an appropriate initial guess of the profiles, and the solver iteratively adjusts the solution at collocation points to satisfy both the differential equations and the boundary conditions. A strict convergence criterion with an absolute error tolerance of 10^{-6} is maintained to ensure numerical accuracy. Mesh refinement and consistency checks are performed to verify smoothness and correct asymptotic behavior of the velocity, temperature, and concentration fields, ensuring reliable and physically meaningful results for the non-Newtonian slip flow with thermal stratification.

3.1 Validation of computed results

The accuracy of the numerical solutions obtained via the `bvp4c` has been validated through systematic comparisons with previously published work of Mir et al. [35]. An excellent agreement is observed when our results are compared against classical and contemporary works across multiple physical regimes. For Newtonian flow, the Nusselt number $\left(Re^{-\frac{1}{2}}Nu_x\right)$ and Sherwood number $\left(Re^{-\frac{1}{2}}Sh_x\right)$ match the values reported by Mir et al. [35] within 0.003%, as demonstrated in Table 1. This comparison, supplemented by cross-verification using MATLAB's `bvp4c`, confirms the robustness of our computational approach and establishes a firm foundation for the novel findings presented in this study.

Table 1. Numerical validation of the Nusselt number $(Re^{-\frac{1}{2}}Nu_x)$ and Sherwood number $(Re^{-\frac{1}{2}}Sh_x)$ in the limiting cases $s_t = 0 = R = s_c$.

Nb		Mir et al. [35]		Present analysis	
Nb	Nt	$(Re^{-\frac{1}{2}}Nu_x)$	$(Re^{-\frac{1}{2}}Sh_x)$	$(Re^{-\frac{1}{2}}Nu_x)$	$(Re^{-\frac{1}{2}}Sh_x)$
0.1	0.1	0.29570	0.18527	0.2957023	0.18527051
0.2	–	0.28845	0.24963	0.28845214	0.24963123
0.3	–	0.28125	0.27103	0.28125327	0.27103214
0.1	0.1	0.29570	0.18527	0.29570231	0.18527324
–	0.2	0.28984	0.06907	0.28984145	0.06907321
–	0.3	0.27419	-0.03954	0.27419327	-0.03954412

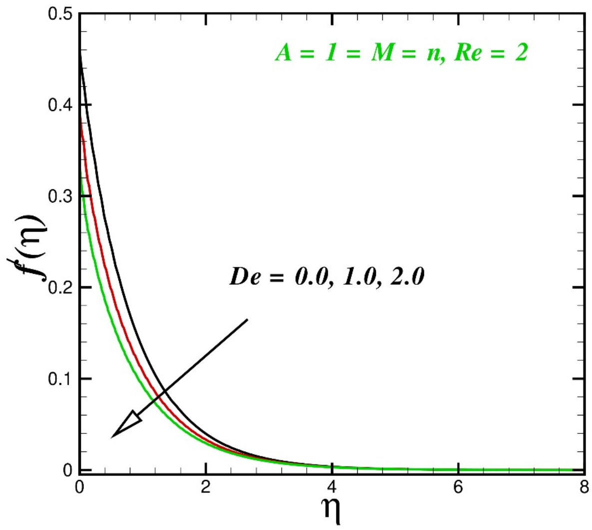

Figure 3. The influence of De on $f'(\eta)$.

4 Results and Discussion

The computed numerical results are graphically displayed via Figures 2–13 for velocity, temperature and concentration profiles. Figures 14–17 display the graphs for skin friction coefficient, local Nusselt number and local Sherwood number.

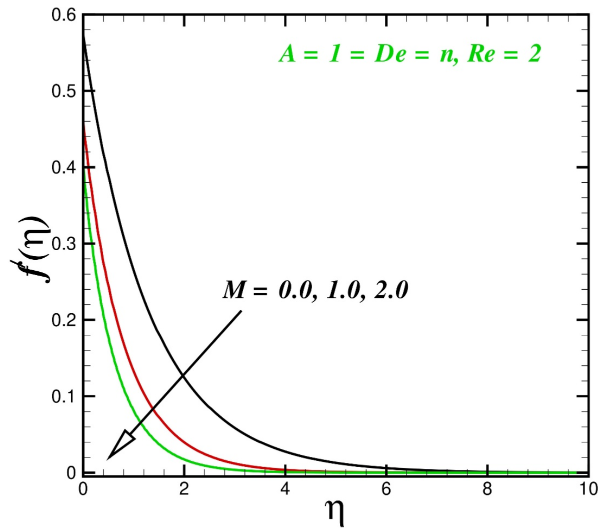

Figure 2. The influence of M on $f'(\eta)$.

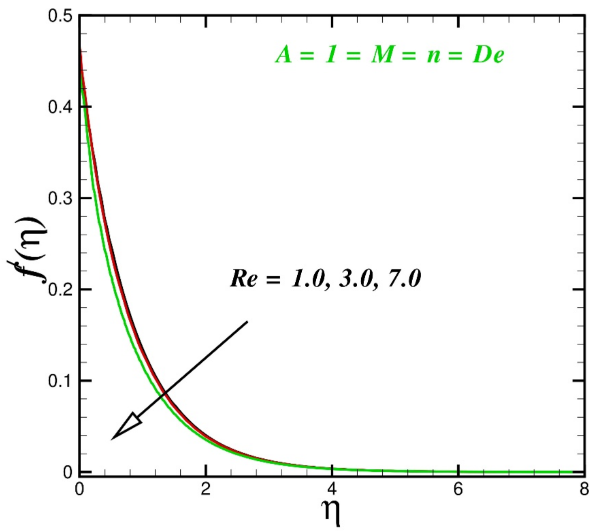

Figure 4. The influence of Re on $f'(\eta)$.

Figure 2 demonstrates the impact of the magnetic parameter M on dimensionless velocity. For the dominant magnetic parameter, there is a decrease in the velocity field. Higher magnetic fields induce Lorentz forces, which cause the velocity field to decay. As a result, horizontal velocity falls.

The influence of Sutterby fluid Deborah number De on the velocity profile is shown in Figure 3. Deborah number is characterized as the proportion of the characteristic time to the time scale of distortion. This implies that the fluid velocity $f'(\eta)$ decreases as the Deborah number De increases.

Figure 4 shows the velocity profile graph with Reynolds number Re. The Reynolds number is an important dimensionless parameter in fluid mechanics that characterizes various flow regimes. It is observed that the velocity profile decreases with increasing values of the Reynolds number Re.

Observing Figure 5, it is found that the velocity profile decreases with increasing values of the velocity slip parameter A.

The influence of Prandtl number Pr on $\theta(\eta)$ is shown in Figure 6. Clearly, $\theta(\eta)$ is reduced for higher values of Pr.

The Prandtl number Pr is the ratio of momentum

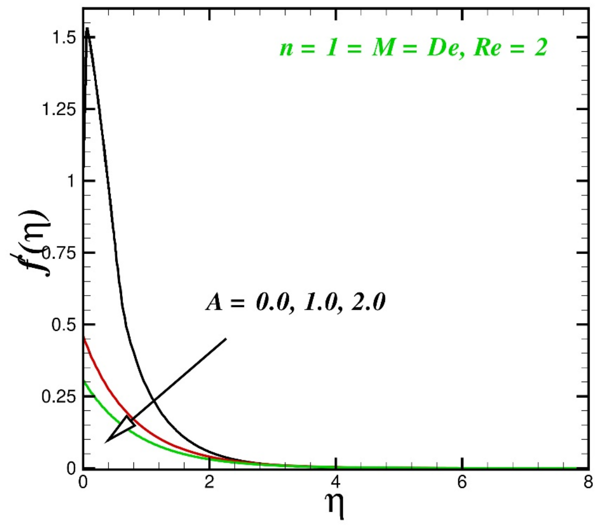

Figure 5. The influence of A on $f'(\eta)$.

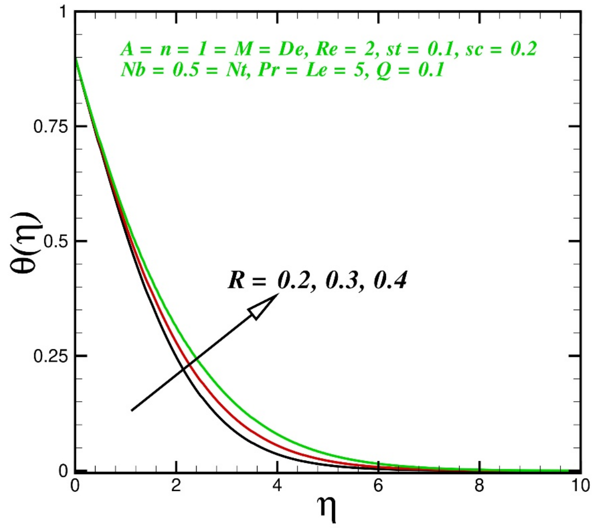

Figure 7. The influence of R on $\theta(\eta)$.

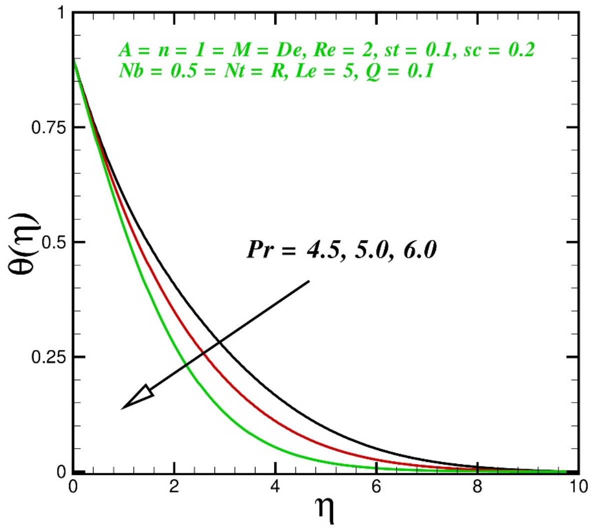

Figure 6. The influence of Pr on $\theta(\eta)$.

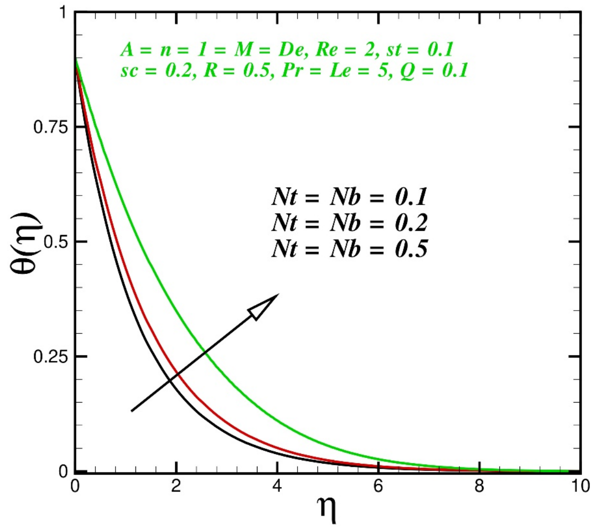

Figure 8. The influence of $Nt = Nb$ on $\theta(\eta)$.

diffusivity to thermal diffusivity in physical terms. For increasing Prandtl numbers, thermal diffusivity dominates and temperature decays.

Figure 7 depicts the temperature profiles for various values of the radiation parameter R. It is observed that both the temperature distribution and the thermal boundary layer thickness increase with increasing R. Physically, a larger radiation parameter enhances the radiative heat flux, leading to greater heating of the working fluid and thus a rise in temperature within the boundary layer.

The effect of Brownian motion and the thermophoresis parameter is shown in Figure 8. The thermal boundary layer thickness grows as the thermophoresis parameter increases, and the temperature gradient at the surface decreases as both Nb and Nt increase. The heat transmission rate at the surface is represented by the local Nusselt number, which drops. As a result, the temperature on the sheet's surface rises. This is owing to the fact that Nt is directly proportional to the fluid's heat transfer coefficient.

Figure 9 is an outline for temperature profile with different values of thermal stratification parameter s_t. The temperature is decreased for higher values of the thermal stratification parameter. It is additionally noticed that the case of prescribed

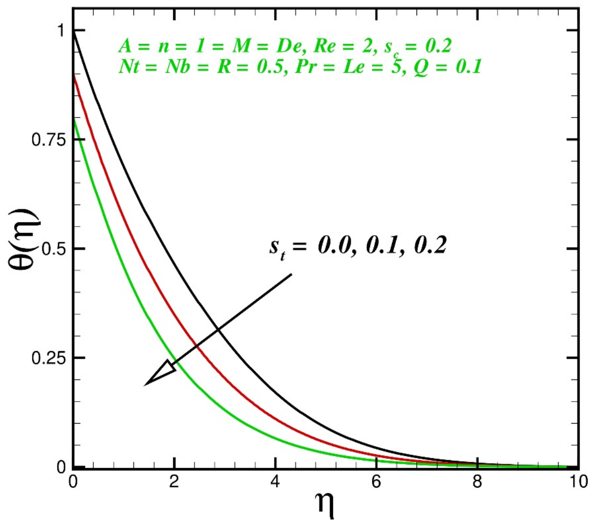

Figure 9. The influence of S_t on $\theta(\eta)$.

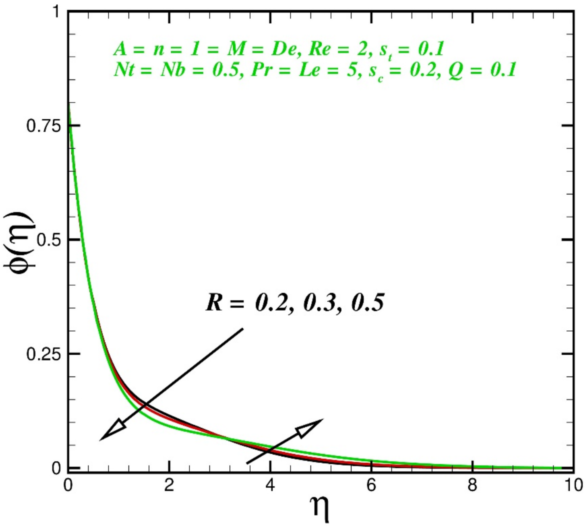

Figure 11. The influence of R on $\varphi(\eta)$.

surface temperature is accomplished when thermal stratification is non-appearance $(s_t = 0)$. Physically, the variation between the surface temperature and the surrounding temperature is lessened for a large value of thermal stratification.

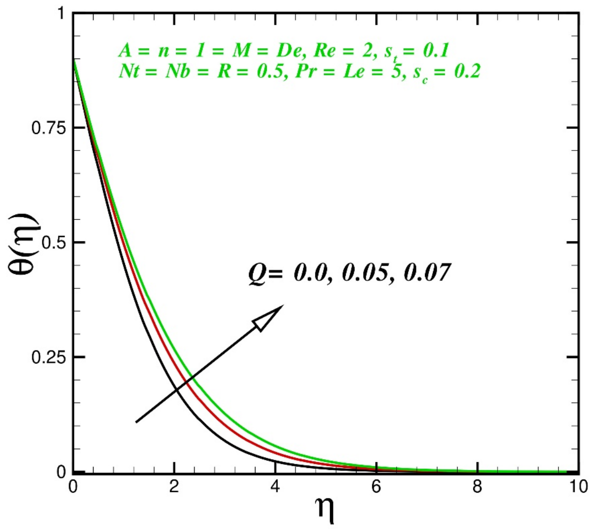

Figure 10. The influence of Q on $\theta(\eta)$.

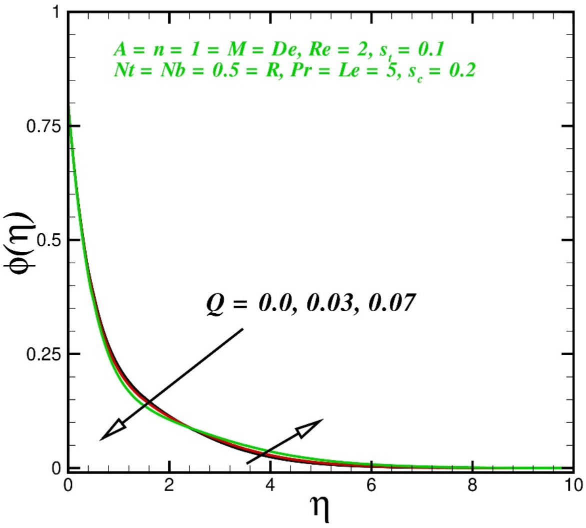

Figure 12. The influence of Q on $\varphi(\eta)$.

The influence of the heat generation/absorption parameter on temperature profiles is depicted in Figure 10. The temperature profiles grow as the heat generation/absorption parameter Q increases, as shown in the graph. This is due to the fact that when the heat generation increases, the fluid's thermal state rises.

Figures 11 and 12 display the variety of thermal radiation parameter R and heat generation/absorption parameter Q on the concentration graph in intervals.

The effect of the solutal stratification parameter s_c on fluid concentration is depicted in Figure 13, where the concentration field decays for the dominating value of the solutal stratification parameter s_c. It can be seen that the concentration is most extreme at $(s_c = 0)$.

Change in local skin friction coefficient $C_f(Re)^{\frac{1}{2}}$ with A when values of M changing from 0 to 2 for classical and Sutterby fluids is shown in Figure 14. It is noticed that the value of skin friction coefficient is higher for Sutterby fluid case, i.e., $De = Re = n = 1.5$, as

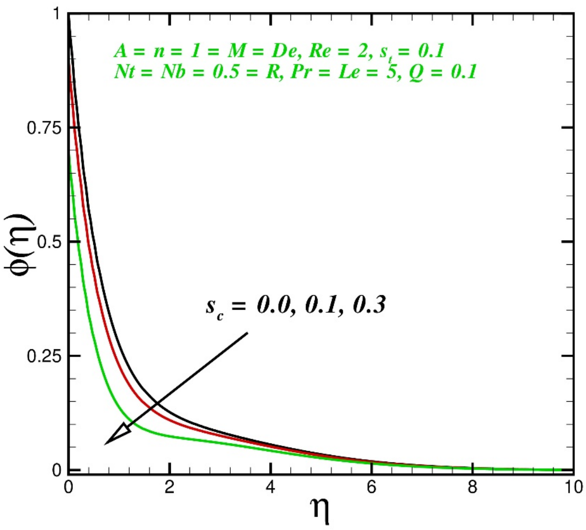

Figure 13. The influence of S_c on $\varphi(\eta)$.

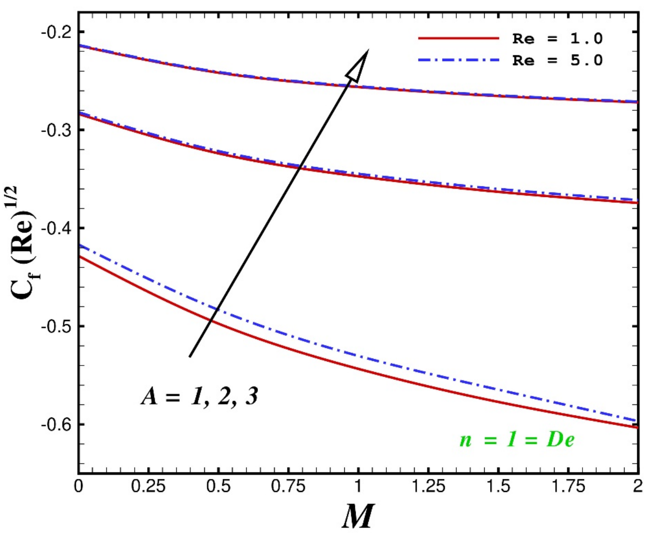

Figure 15. The influence of A on $C_f(Re_x)^{\frac{1}{2}}$.

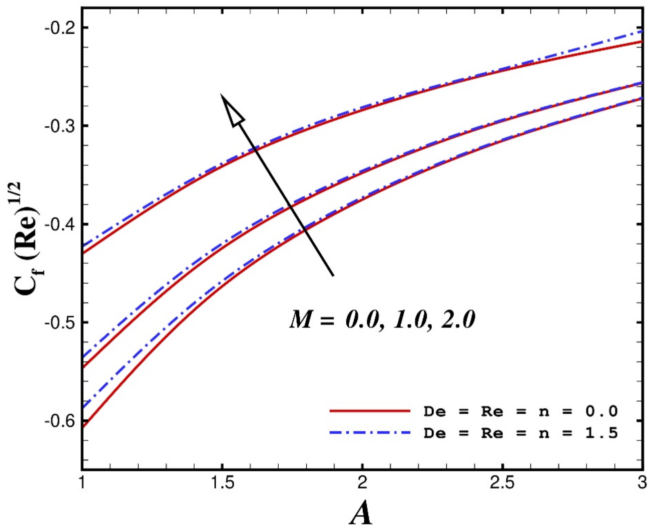

Figure 14. The influence of M on $C_f(Re_x)^{\frac{1}{2}}$.

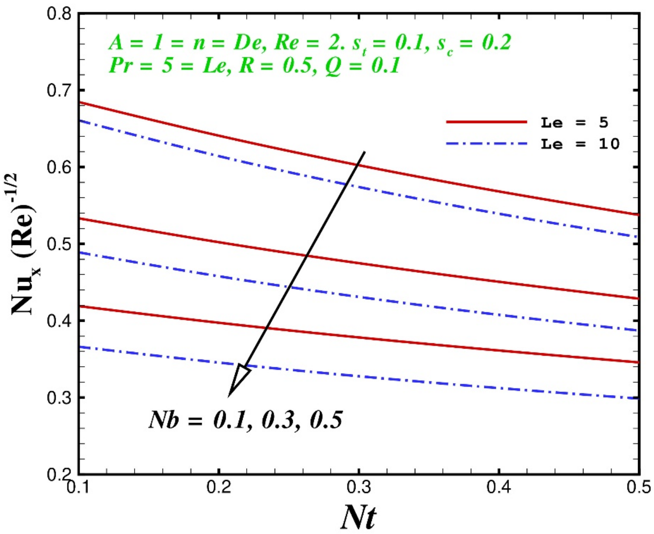

Figure 16. The influence of Nt and Nb on $Nu_x(Re_x)^{-\frac{1}{2}}$.

compared with classical case, i.e., $De = Re = n = 0$. It is outstanding that the fluid for the Sutterby fluid diminishes to the Newtonian fluid flow by considering $M = De = Re = 0$.

Figure 15 shows the impact of velocity slip parameter A on skin friction coefficient against magnetic parameter M for both cases ($Re = 1$, $Re = 5$). As the values of velocity slip parameter A increase, the value of skin friction coefficient increases; however, as the values of magnetic parameter M increase, the graph of skin friction coefficient diminishes, and the boundary layer thickness as well.

Figure 16 shows the impact of both the Brownian motion parameter Nb and thermophoresis parameter Nt on local Nusselt number $Nu_x(Re_x)^{-\frac{1}{2}}$ for both cases, i.e., $Le = 5$ and $Le = 10$. As the values of the Brownian motion parameter Nb increase, the local Nusselt number decreases; however, as the values of thermophoresis parameter Nt increase, the chart of local Nusselt number diminishes, and the thermal boundary layer thickness as well.

Figure 17 also portrays the variation of local Sherwood number $Sh_x(Re_x)^{-\frac{1}{2}}$ in response to a change in Brownian motion parameter Nb for cases $Le = 5$ and $Le = 10$. The graph shows that the local Sherwood number increases as Nb parameters increase, but it

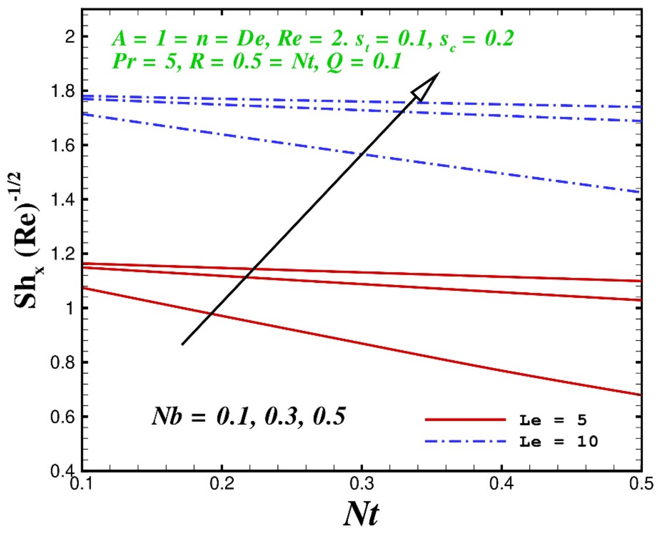

Figure 17. The influence of Nt and Nb on $Sh_x(Re_x)^{\frac{1}{2}}$.

diminishes with an increase in Nt.

5 Conclusion

This study presents a comprehensive analysis of heat transport characteristics in a Sutterby nanofluid subject to heat generation/absorption and slip boundary conditions. The influence of pertinent physical parameters on velocity, temperature, concentration distributions, and engineering quantities of interest has been systematically examined. The principal findings are summarized as follows.

The application of a magnetic field significantly suppresses the fluid motion. An increase in the magnetic parameter M reduces the velocity profiles and thins the momentum boundary layer due to the resistive Lorentz force generated in the electrically conducting fluid. The surface velocity decreases with increasing values of the Deborah number De and Reynolds number Re. Higher Deborah numbers intensify the elastic behavior of the Sutterby fluid, thereby resisting deformation and reducing near-wall velocity.

The thermal boundary layer thickness decreases with increasing thermal stratification parameter s_t and Prandtl number Pr. Larger Prandtl numbers correspond to lower thermal diffusivity, restricting heat propagation within the fluid. Thermal stratification further weakens thermal interaction between the wall and the fluid, leading to reduced temperature distribution. In contrast, the radiation parameter R and heat generation parameter Q enhance the thermal field.

The concentration boundary layer thickness decreases with increasing solutal stratification parameter s_c, indicating reduced nanoparticle diffusion from the surface. Finally, the skin friction coefficient C_f is found to be higher for the Sutterby fluid compared to the classical Newtonian fluid when the magnetic parameter increases. This outcome reflects the combined influence of viscoelastic rheology and magnetic damping, which enhances wall shear stress and mechanical resistance.

Overall, the present investigation provides valuable insights into the thermal and flow control of non-Newtonian nanofluids under electromagnetic and slip effects. The results are relevant to engineering applications such as polymer extrusion, cooling of electronic devices, biomedical transport systems, and magnetically controlled thermal processing technologies.

Data Availability Statement

Data will be made available on request.

Funding

This work was supported without any funding.

Conflicts of Interest

The authors declare no conflicts of interest.

AI Use Statement

The authors declare that no generative AI was used in the preparation of this manuscript.

Ethical Approval and Consent to Participate

Not applicable.

References

[1] Choi, S. U. (1995, November). Enhancing thermal conductivity of fluids with nanoparticles. In *ASME international mechanical engineering congress and exposition* (Vol. 17421, pp. 99-105). American Society of Mechanical Engineers. [CrossRef]

[2] Xuan, Y., & Li, Q. (2000). Heat transfer enhancement of nanofluids. *International Journal of Heat and Fluid Flow, 21*(1), 58–64. [CrossRef]

[3] Buongiorno, J. (2006). Convective transport in nanofluids. *Journal of Heat Transfer, 128*(3), 240–250. [CrossRef]

[4] Kuznetsov, A. V., & Nield, D. A. (2010). Natural convective boundary-layer flow of a nanofluid past a vertical plate. *International Journal of Thermal Sciences, 49*(2), 243-247. [CrossRef]

[5] Makinde, O. D., & Aziz, A. (2011). Boundary layer flow of a nanofluid past a stretching sheet with a convective boundary condition. *International Journal of Thermal Sciences, 50*(7), 1326-1332. [CrossRef]

[6] Mustafa, M., Hayat, T., Pop, I., Asghar, S., & Obaidat, S. (2011). Stagnation-point flow of a nanofluid towards a stretching sheet. *International Journal of Heat and Mass Transfer, 54*(25-26), 5588-5594. [CrossRef]

[7] Ibrahim, W., Shankar, B., & Nandeppanavar, M. M. (2013). MHD stagnation point flow and heat transfer due to nanofluid towards a stretching sheet. *International journal of heat and mass transfer, 56*(1-2), 1-9. [CrossRef]

[8] Hamad, M. A. A., & Ferdows, M. (2012). Similarity solution of boundary layer stagnation-point flow towards a heated porous stretching sheet saturated with a nanofluid with heat absorption/generation and suction/blowing: a Lie group analysis. *Communications in Nonlinear Science and Numerical Simulation, 17*(1), 132-140. [CrossRef]

[9] Hayat, T., Imtiaz, M., & Alsaedi, A. (2016). Magnetohydrodynamic flow of nanofluid over permeable stretching sheet with convective boundary conditions. *Thermal science, 20*(6), 1835-1845. [CrossRef]

[10] Pop, I., Roşca, N. C., & Roşca, A. V. (2018). MHD stagnation-point flow and heat transfer of a nanofluid over a stretching/shrinking sheet with melting, convective heat transfer and second-order slip. *International Journal of Numerical Methods for Heat & Fluid Flow, 28*(9), 2089–2110. [CrossRef]

[11] Aly, E. H., & Pop, I. (2020). MHD flow and heat transfer near stagnation point over a stretching/shrinking surface with partial slip and viscous dissipation: Hybrid nanofluid versus nanofluid. *Powder Technology, 367*, 192–205. [CrossRef]

[12] Waqas, H., Farooq, U., Liu, D., Abid, M., Imran, M., & Muhammad, T. (2022). Heat transfer analysis of hybrid nanofluid flow with thermal radiation through a stretching sheet: A comparative study. *International Communications in Heat and Mass Transfer, 138*, 106303. [CrossRef]

[13] Iqbal, J., & Abbasi, F. M. (2025). Convective heat transfer analysis for magnetohydrodynamics Reiner–Philippoff nanofluid flow over a curved stretching surface: non-similar solution. *Multidiscipline Modeling in Materials and Structures, 21*(2), 405-424. [CrossRef]

[14] Hashim, Bouzgarrou, S., Rehman, S., & Sabi, E. (2023). Thermodynamic analysis of Powell-Eyring-blood hybrid nanofluid through vertical stretching sheet with interface slip and melting heat. *Results in Engineering, 20*, 101644. [CrossRef]

[15] Turkyilmazoglu, M. (2024). Two models on the unsteady heat and fluid flow induced by stretching or shrinking sheets and novel time-dependent solutions. *Journal of Heat and Mass Transfer, 146*(10), 101802. [CrossRef]

[16] Hassani, M., Tabar, M. M., Nemati, H., Domairry, G., & Noori, F. (2011). An analytical solution for boundary layer flow of a nanofluid past a stretching sheet. *International Journal of Thermal Sciences, 50*(11), 2256-2263. [CrossRef]

[17] Khan, W. A., & Pop, I. (2010). Boundary-layer flow of a nanofluid past a stretching sheet. *International journal of heat and mass transfer, 53*(11-12), 2477-2483. [CrossRef]

[18] Bhattacharyya, K., Mukhopadhyay, S., & Layek, G. C. (2011). MHD boundary layer slip flow and heat transfer over a flat plate. *Chinese Physics Letters, 28*(2), 024701. [CrossRef]

[19] Waseem, F., Sohail, M., & Singh, A. (2024). Entropy analysis of three-dimensional stretched magnetized hybrid nanofluid with thermal radiation and heat generation. *BioNanoScience, 14*(2), 547-565. [CrossRef]

[20] Waseem, F., Sohail, M., Ilyas, N., Awwad, E. M., Sharaf, M., Khan, M. J., & Tulu, A. (2024). Entropy analysis of MHD hybrid nanoparticles with OHAM considering viscous dissipation and thermal radiation. *Scientific Reports, 14*(1), 1096. [CrossRef]

[21] Rashidi, M. M., Ganesh, N. V., Hakeem, A. A., & Ganga, B. (2014). Buoyancy effect on MHD flow of nanofluid over a stretching sheet in the presence of thermal radiation. *Journal of Molecular liquids, 198*, 234-238. [CrossRef]

[22] Ibrahim, W., & Shankar, B. (2013). MHD boundary layer flow and heat transfer of a nanofluid past a permeable stretching sheet with velocity, thermal and solutal slip boundary conditions. *Computers & Fluids, 75*, 1-10. [CrossRef]

[23] Andersson, H. I. (2002). Slip flow past a stretching surface. *Acta Mechanica, 158*(1), 121-125. [CrossRef]

[24] Wang, C. Y. (2002). Flow due to a stretching boundary with partial slip—an exact solution of the Navier–Stokes equations. *Chemical Engineering Science, 57*(17), 3745-3747. [CrossRef]

[25] Wang, C. Y. (2006). Stagnation slip flow and heat transfer on a moving plate. *Chemical Engineering Science, 61*(23), 7668-7672. [CrossRef]

[26] Wu, L. (2008). A slip model for rarefied gas flows at arbitrary Knudsen number. *Applied Physics Letters, 93*(25), 053103. [CrossRef]

[27] Fang, T., Zhang, J., & Yao, S. (2009). Slip MHD viscous flow over a stretching sheet–an exact solution.

Communications in Nonlinear Science and Numerical Simulation, *14*(11), 3731-3737. [CrossRef]

[28] Hayat, T., Qasim, M., & Mesloub, S. (2011). MHD flow and heat transfer over permeable stretching sheet with slip conditions. *International Journal for Numerical Methods in Fluids*, *66*(8), 963-975. [CrossRef]

[29] Aziz, A. (2010). Hydrodynamic and thermal slip flow boundary layer over a flat plate with constant heat flux boundary condition. *Communications in Nonlinear Science and Numerical Simulation*, *15*(3), 573–580. [CrossRef]

[30] Fang, T., Yao, S., Zhang, J., & Aziz, A. (2010). Viscous flow over a shrinking sheet with a second order slip flow model. *Communications in Nonlinear Science and Numerical Simulation*, *15*(7), 1831-1842. [CrossRef]

[31] Nandeppanavar, M. M., Vajravelu, K., Abel, M. S., & Siddalingappa, M. N. (2012). Second order slip flow and heat transfer over a stretching sheet with non-linear Navier boundary condition. *International Journal of Thermal Sciences*, *58*, 143-150. [CrossRef]

[32] Turkyilmazoglu, M. (2012). Exact analytical solutions for heat and mass transfer of MHD slip flow in nanofluids. *Chemical Engineering Science*, *84*, 182-187. [CrossRef]

[33] Alsaedi, A., Awais, M., & Hayat, T. (2012). Effects of heat generation/absorption on stagnation point flow of nanofluid over a surface with convective boundary conditions. *Communications in Nonlinear Science and Numerical Simulation*, *17*(11), 4210-4223. [CrossRef]

[34] Sutterby, J. L. (1965). Laminar converging flow of dilute polymer solutions in conical sections. II. *Transactions of the Society of Rheology*, *9*(2), 227-241. [CrossRef]

[35] Mir, N. A., Farooq, M., Rizwan, M., Ahmad, F., Ahmad, S., & Ahmad, B. (2020). Analysis of thermally stratified flow of Sutterby nanofluid with zero mass flux condition. *Journal of Materials Research and Technology*, *9*(2), 1631-1639. [CrossRef]

Dr. Hashim is a distinguished scholar in the field of Applied Mathematics, with a specialized focus on fluid mechanics and heat transfer. He earned his Ph.D. in Applied Mathematics from Quaid-I-Azam University, Islamabad in 2018. (Email: hashim@uoh.edu.pk)